SAND78-0336
Unlimited Release

The Thomson Parabola Ion Analyzer

Michael A. Gusinow, Maurice M. Dillon, Grant J. Lockwood, Laurence E. Ruggles

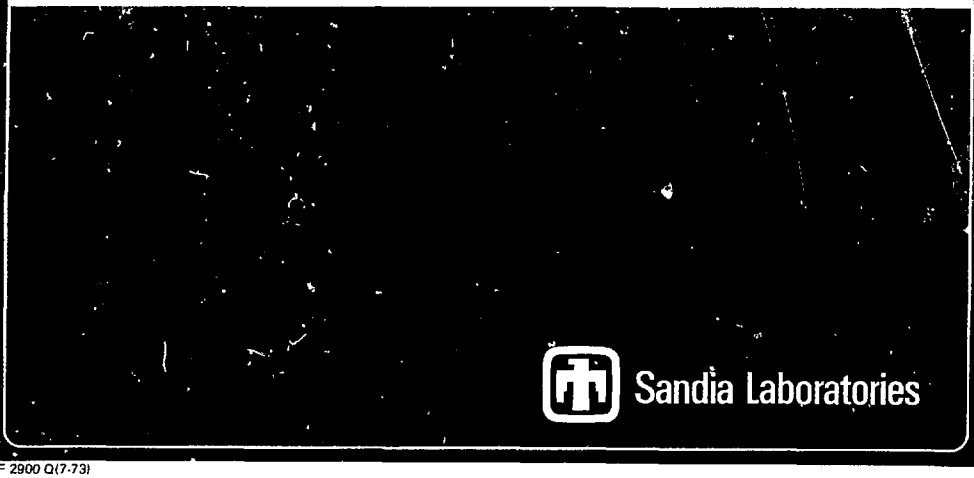

SF 2900 Q(7-73)

SAND78-0336
Unlimited Release
Printed March 1978

THE THOMSON PARABOLA ION ANALYZER

Michael A. Gusinow
Maurice M. Dillon
Plasma and Laser Physics Division 5215

Grant J. Lockwood
Laurence E. Ruggles
Beam Source Application Division 5232

Sandia Laboratories
Albuquerque, NM 87185

ABSTRACT

A Thomson parabola ion analyzer is calibrated for ion energy and ionic charge to mass ratio determination. Characteristic of this device which influence its operation are discussed.

CONTENTS

THE THOMSON PARABOLA ION ANALYZER

Introduction

This report describes the operation and calibration of a Thomson-parabola ion analyzer. This instrument is capable of measuring the ionic charge states present in a plasma. It also exhibits energy dispersion which in principle makes it possible to determine the distribution of energy among those ions reaching the analyzer. The device has been discussed by Olsen, et al[1] regarding its use with laser-produced plasmas. The effect of an ambient gas on the utility of this instrument has been discussed by Pearlman and Matzen.[2] The detector in the present device is a Bendix channeltron electron multiplier array (CEMA). The output of the CEMA is used to excite a phosphor, the output of which is then recorded on film. The output of the CEMA-phosphor does not readily allow for calibration to ascertain the absolute (or relative) number of particles impinging upon it. Consequently, with a CEMA one must be content to determine charge states and certain aspects of the energy of the sampled plasma. Absolute measurements of the ion energy distribution can be made by utilizing an appropriate detector.[3] There are a variety of plasma ion detectors available; we mention one of them because of certain similarities to the Thomson parabola in its applications to laser-produced plasmas. The electrostatic ion analyzer described by Decoste and Ripin[4] and by Lockwood[5] has the advantage over the present instrument of giving the time-of-arrival response[6] of the various charge states as well as their energy distribution.

Theory of Operation

A schematic representation of the device is shown in Figure 1.

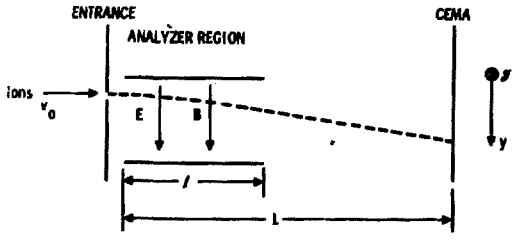

$$\Delta y = \frac{eZ\mathcal{E}l}{Mv_0^2}\left|1 - \frac{l}{2L}\right| \quad (1)$$

$$\Delta y = \frac{eZBl}{Mv_0}\left|1 - \frac{l}{2L}\right| \quad (2)$$

Figure 1. A Schematic Representation for the Analysis of the Thomson Parabola Analyzer

The equations of motion governing an incoming ion of charge Z, atomic mass A, and velocity v_o are:

$$\ddot{x} = -\omega_H v_z \tag{3}$$

$$\ddot{y} = \frac{Ze}{M}\mathcal{E} \tag{4}$$

$$\ddot{z} = \omega_H v_x \tag{5}$$

where $\omega_H = ZeB/M$, M ($M = Am_o$, where m_o is the proton mass) is the atomic mass, e is the electronic charge, B and $\mathcal{E}$ are the applied magnetic and electric fields respectively. These equations are easily solved to find the trajectory of the particle in the analyzer region (length ℓ). Upon leaving the analyzer region, the particle is in free flight and impinges upon the CEMA where it is detected. The locus of ions with a constant charge-to-mass ratio for various energies is given in the equations in Figure 1. The pattern described is a parabola in the y-z plane given by

$$(\Delta y)\left(\frac{\ell LB^2 e}{m_o \mathcal{E}}\right)\left(\frac{Z}{A}\right) = (\Delta_z)^2 \tag{6}$$

The coordinate system and units along the axis for the instrument used in this work are shown in Figure 2 (axes labeled according to Eqs. 1 and 2).

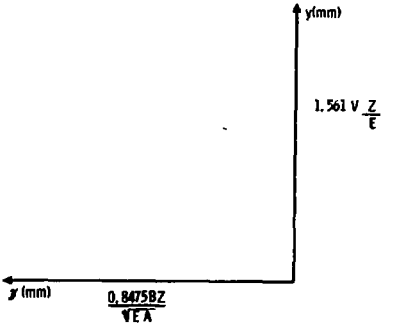

Figure 2. The Coordinate System Used for Analysis of the Ion Traces Observed at the Analyzer Exit Face

For a particular parabola (given Z/A) those ions farthest from the origin correspond to lower entrance energies than those closer to the origin. The above equations assume $\omega_H \ell / v_o << 1$ and are correct to first order. The velocity in the x-direction to first order does not change as the particle traverses the analyzer region. The error involved in not going to higher orders is less than 1 percent for typical laser-plasma conditions.

The above is derived for single particle behavior. The effects of fringing fields and space charge on the particle trajectories will be dealt within this report.

Apparatus and Procedure

The analyzer to be calibrated is shown schematically in Figure 1 where ℓ = 150 mm, L = 333 mm and the plate spacing was 12.4 mm. Note that the electric field plates were made of soft iron and served as the magnetic pole pieces for the magnetic field. The field was obtained by placing permanent magnets on both sides of the analyzer (outside the vacuum housing) at the position of the internal pole pieces, and was varied by changing the spacing between the externally applied magnets and the pole pieces by the use of aluminum spacers.

The Sandia Laboratories 100 kV ion accelerator was used in this study. The ions were produced in an rf ion source using H_2, Ne, and Ar gas. The source provided ions from charge 1 to 3 depending on the gas used. The accelerator delivered a beam of magnetically analyzed ions (having an energy spread of less than 34 eV) to the analyzer. The beam energy was determined to within a 1.0% accuracy by measuring the terminal potential with a voltage divider and correcting for ion-source potentials. Due to charge transfer from collisions with background gas molecules in the accelerator between the ion beam analyzing magnet and the Thomson parabola analyzer, the incident beam contained a small fraction of ions of lower charge state than those selected by the analyzing magnet. The small neutral component produced an image on the recording film corresponding to zero deflection. This image was used as the reference from which the deflections were measured. In the cases of selected doubly and triply charged ions, the lower charge states allow for simultaneous measurement of the deflection of various charge to mass ratio ions with a common velocity.

The following procedure was used in the calibration. For each selected charge-to-mass ratio ion beam at a given energy (i.e., velocity) the beam was pulsed on for a time sufficient to obtain a good film exposure. This was repeated as the electric and magnetic fields applied to the analyzer were varied in discrete steps. The electric field was varied by changing the voltage applied in the electric field plates. The magnetic field was varied by use of the aluminum spacers previously mentioned.

Results and Discussion

During the course of this work, measurements were made for ions of various charge-to-mass ratios from 1:1 to 1:40. The velocity range covered was from 2.17×10^7 cm/s to 4.38×10^8 cm/s. Table I lists the velocities of the various charge-to-mass ratios of the ion species used.

TABLE I

Charge-To-Mass Ratio and Velocity of Ions Used in Calibration

Z/A / Vel. cm/s	1/1 (H^+)	1/2 (H_2^+)	1/10 (Ne^{2+})	3/40 (Ar^{3+})	1/20 (Ne^+,Ar^{2+})	1/40 (Ar^+)
	1.95×10^8	1.70×10^8	8.87×10^7	1.20×10^8	2.17×10^7	2.19×10^7
	3.10×10^8		1.07×10^8		3.09×10^7	4.90×10^7
	4.38×10^8				4.38×10^7	6.92×10^7
					6.20×10^7	
					7.58×10^7	
					8.74×10^7	
					9.77×10^7	
					9.78×10^7	
					1.07×10^8	

Typical data obtained during these measurements are shown in Figures 3 and 4. Figure 3 presents the results obtained for a 1.95×10^8 cm/s (19.92 keV) H^+ incident beam.

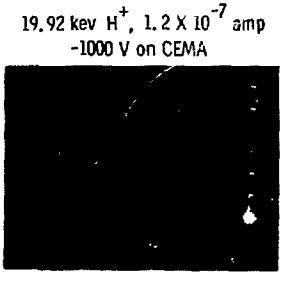

Figure 3. The Calibration Output Using 19.92 keV H^+ Ions for Various Electric Fields

The magnetic field was kept at zero and the electric field was varied by changing the plate voltage in six 80-V steps from 0 to 480 volts. The voltages listed are the total voltage differences between the plates. This was accomplished by applying -(1/2) V to one plate and +(1/2) V to the other plate. The results are a series of seven exposures along the electric (y) axis. The lowest (brightest) spot defines the origin and occurs in the case of zero electric and magnetic fields. This is because the beam strikes this location each time it is pulsed on. Each of the other six exposures appear to consist of two spots. We believe that this effect is caused by a surface charge on the CEMA face. For CEMA voltages less than -1000 V only a single spot occurred. Figure 4 shows the results for incident beams of 1.70 x 10^8 cm/s (30.14 keV) H_2^+, 2.17 x 10^7 cm/s (4.94 keV) Ne^+ and 2.19 x 10^7 cm/s (10.02 keV) Ar^+ respectively.

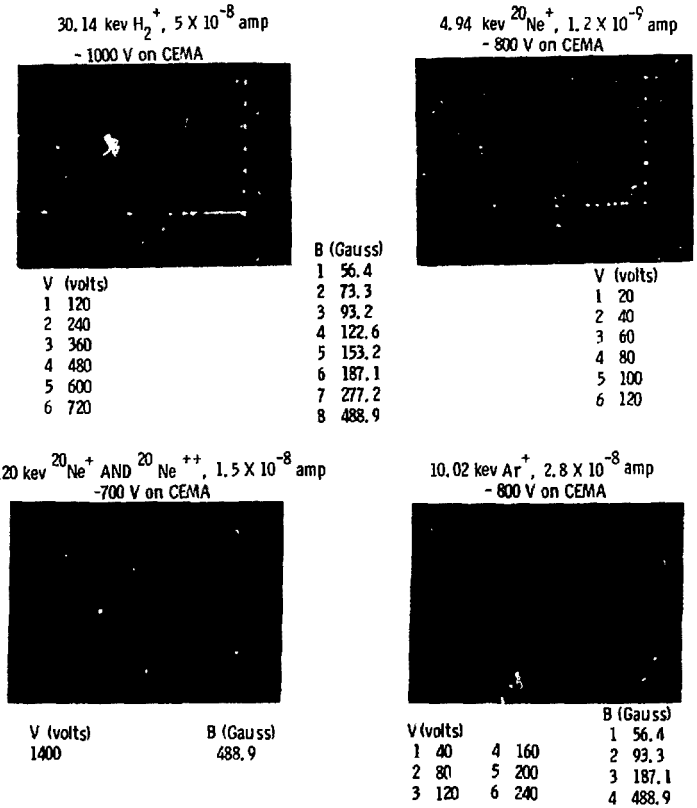

Figure 4. The Calibration Output for Various Ions and Energies

In these cases, the electric field was first varied in steps with a zero magnetic field; then the magnetic field was varied in steps with a zero electric field. As in Figure 3, the deflections due to the varied electric field appear as spots along the y axis. The deflections due to the varied magnetic field appear as spots along the y axis. Also shown in Figure 4 are the results for an incident Ne^{2+} beam with a velocity of 1.07×10^8 cm/s (120 keV). As explained earlier, due to charge transfer there was also a small beam of Ne^{+} at 1.07×10^8 cm/s. Thus with zero magnetic field and 1400 V on the electric field plates, two deflected spots appear along the y axis. The upper spot is due to the Ne^{+2} while the lower spot is due to the Ne^{+1}. Then with the electric field at zero, a magnetic field was applied resulting in the two spots along the y axis. Finally both fields were applied at the same time giving rise to the two off-axis spots.

When the measured deflections due to the electric field are compared with those predicted by Eq. 1 the average difference is 1.98 percent for energies of 40 keV and higher. However, the difference increases as the energy is lowered, reaching a value of 8.12 percent at 4.94 keV. It is believed that this is caused mainly by the electric field due to the negative voltage applied to the front of the CEMA.

A mapping of the magnetic field with a gauss meter indicated an average variation of approximately 3 percent and a peak of 11 percent. From the measured magnetic deflections with the various spacers, effective magnetic fields can be inferred. These are shown in Table II.

TABLE II

Effective Magnetic Fields Determined From Calibration

Spacer Number	Spacer Thickness (cm)	Magnetic Field (Gauss)
1	3.810	56.4 (±5.4%)
2	3.175	73.3 (±3.9%)
3	2.540	93.2 (±4.0%)
4	1.905	122.6 (±5.6%)
5	1.587	153.2 (±2.0%)
6	1.270	187.1 (±2.9%)
7	0.635	277.2 (±5.8%)
8	0	488.9 (±2.8%)

The average precision is taken to be 4 percent. Using the results of these calibrations, relations can be obtained among deflections in the electric and magnetic field to the charge-to-mass ratio and the velocity of the incident ions. Using Eqs. 1 and 2 the following occurs:

$$\frac{Z}{A} = 2.17 \frac{(\Delta y)^2}{\Delta y} \left(\frac{V}{B^2}\right) \tag{7}$$

and

$$v_o = 8.06 \times 10^7 \left(\frac{\ell_z}{\Delta y}\right)\left(\frac{V}{B}\right) \text{cm/sec} \tag{8}$$

where Z/A is the ionic charge per amu (more specifically Z is the charge state of the ion), Δy and Δy are in mm, V is in volts, and B is in Gauss. B is the effective magnetic field and ±4 percent precision is associated with it. We ascribe an average precision of ±3 percent to an effective deflection plate voltage (aside from the systematic errors previously noted). Consequently, the charge-to-mass ratio (Eq. 7) can be determined with an uncertainty of ±11 percent, while the velocity can be determined to within ±7 percent. Many laser-plasma experiments deal with a specific target material and hence A is unambiguously known. An important quantity is E/Z where E is the kinetic energy of the Z^{th} charge state entering the analyzer region. In this case (from Figure 2),

$$\frac{E}{Z} = 1.561 \left(\frac{V}{\Delta y}\right) \text{keV} \tag{9}$$

The energy of the various charge states observed can be determined to within ±3 percent.

The Thomson parabola ion analyzer has been calibrated for use with laser experiments to study expanding plasmas produced by laser interaction with a solid target. In this case the principal mass component (A) of the plasma is known; thus, one can obtain ionic charge and energy information. Figure 5 is a typical trace from an experiment using an Aℓ target and a 50 ps, 900 mJ, 1.06 μ laser.

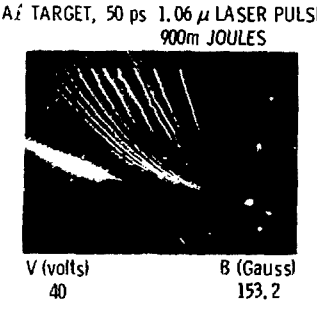

Figure 5. A Typical Thomson Parabola Analyzer Output for an Expanding Aℓ Plasma Produced With a 50 ps, 900 mJ, 1.60 μ Laser

Various stages of ionization of the Al are observed (Z = 1 through 11) as well as impurities. The most notable impurity is H^+, the brightest trace in the left-hand corner. The absence of the traces towards the origin is indicative of an upper energy cutoff in the expanding plasma.

References

1. J. N. Olsen, G. W. Kuswa, E. D. Jones, J. A. P., 44, 2276, 1973.

2. J. Pearlman and M. K. Matzen, paper 10H4, 19th Annual Meeting of the Division of Plasma Physics, 1977.

3. F. Young and G. H. McCall, paper 5H9, ibid, 19th Annual Meeting of the Division of Plasma Physics, 1977.

4. R. DeCoste and B. H. Ripin, Rev. Sci. Instru., 48, 232, 1977.

5. G. J. Lockwood, Sandia Research Report, SC-RR-70-583, 1970.

6. E. D. Jones suggested privately circa 1975 that a framing camera be utilized to look at the CEMA response as a function of time during plasma expansion.